The Meteoritical Society

Meteoritics & Planetary Science 42, Nr 1, 131–148 (2007)
Abstract available online at http://meteoritics.org

Phase equilibrium investigations of the Adirondack class basalts from the Gusev plains, Gusev crater, Mars

Anna G. MONDERS, Etienne MÉDARD*, and Timothy L. GROVE

Department of Earth, Atmospheric, and Planetary Sciences, Massachusetts Institute of Technology, 77 Massachusetts Avenue, Building 54-1218, Cambridge, Massachusetts 02139, USA
*Corresponding author. E-mail: emedard@mit.edu

(Received 19 May 2006; revision accepted 11 November 2006)

Abstract–Phase equilibrium experiments have been performed on a synthetic analog of the Gusev plains basalt composition from the Spirit landing site on Mars. Near-liquidus phase relations were determined over the pressure range of 0.1 to 1.5 GPa and at temperatures from 1125 to 1390 °C in a piston cylinder apparatus and 1 atm gas mixing furnace. The composition is multiply saturated with olivine, orthopyroxene, and spinel near its liquidus at 1320 °C and 1.0 GPa, or 85 km depth on Mars, placing an upper limit constraint on the thickness of the Martian lithosphere at the time of eruption. Our experimental work suggests that the Gusev basalts are anhydrous batch melts of a primitive Martian mantle similar to the composition estimated by Dreibus and Wänke (1984). The temperature of multiple saturation indicates the persistence of high mantle potential temperatures on Mars, similar to those on the modern Earth, until at least the very latest Noachian (3.7 Ga). These high mantle temperatures would be responsible for persistent basaltic volcanism throughout the southern highlands during the first billion years of Mars's history. The source for Gusev basalts differs strongly from the source for shergottite meteorites, reinforcing the idea of the absence of global mantle convection and mixing on Mars. The existence of a relatively primitive mantle reservoir requires that at least part of the mantle underwent little modification during early planetary differentiation.

INTRODUCTION

Until recently, the only information on the composition of igneous rocks on Mars and Martian magmatic processes came from shergottite-nakhlite-chassignite (SNC) meteorites (McSween 2002). With the exception of one ancient sample, the pyroxenite cumulate Allan Hills 84001 (Mittlefehldt 1994), these meteorites are young magmatic rocks thought to have been ejected through meteoritic impact from the volcanic areas of Tharsis or Elysium (McSween 1994). Most of these rocks contain accumulated crystals and therefore do not represent liquid compositions, and most are derived from evolved liquids that have experienced varying extents of fractional crystallization. One notable exception is that of several olivine shergottites, for example, Yamato-980459 (Greshake et al. 2004), that have remarkable primitive characteristics (high Mg/[Mg + Fe], rich in olivine). Rocks were analyzed by the Mars Pathfinder mission using the alpha particle X-ray spectrometer (APXS), but the analyzed compositions represent extremely evolved and differentiated andesitic magmas as well (Minitti and Rutherford 2000). Thus, it has been difficult to characterize Martian mantle processes and major element characteristics of Martian mantle source regions.

Basaltic rocks have recently been described from the Spirit landing site at Gusev crater (McSween et al. 2004). These dark, fine-grained, vesicular rocks contain 25% olivine megacrysts (McSween et al. 2006a) and were observed on the floor of Gusev crater during the first 155 sols of Spirit's mission before reaching the Columbia Hills. Three rocks named Humphrey, Adirondack, and Mazatzal have been analyzed and classified by Squyres et al. (2006) as Adirondack class; they will be referred to in this paper as Gusev basalts. Chemical analyses of abraded surfaces of these samples by APXS are consistent with primitive basalts, with an average of 11 wt% MgO (McSween et al. 2006a) (Table 1). There is debate about whether the olivine megacrysts observed in Adirondack, Humphrey, and Mazatzal are actual phenocrysts that crystallized in situ or whether they represent an accumulation of crystals by settling in the lower portion of the cooling unit. In this paper, we assume, after McSween et al. (2006a), that Gusev basalts

Table 1. Composition of Gusev basalts and starting materials.

Oxide (wt%)[a]	Recalibrated data[b]	Experimental composition[c]	Spinel-free experimental composition[d]	Preliminary composition[e]
SiO_2	45.87	46.85	47.25	45.96
TiO_2	0.55	0.48	0.48	0.49
Al_2O_3	10.58	10.69	10.63	11.13
Cr_2O_3	0.63	0.79	0.36	0.58
FeO*	18.92	18.91	18.87	17.12
MnO	0.43	0.43	0.43	0.39
MgO	11.04	11.46	11.47	12.26
CaO	8.10	8.02	8.09	7.67
Na_2O	2.37	1.77	1.79	2.90
K_2O	0.08	0.06	0.06	0.06
P_2O_5	0.59	0.56	0.56	0.59
FeS	0.84	–	–	0.83

[a]Compositions have been renormalized to 100%.
[b]Average of the compositions of Humphrey, Adirondack, and Mazatzal reported in McSween et al. (2006a).
[c]Average estimated composition of piston cylinder runs that contain only spinel as a crystalline phase.
[d]Average composition of glasses in piston cylinder runs that contain only spinel as a crystalline phase.
[e]Average of the compositions of Adirondack, Humphrey, and Mazatzal as initially reported in McSween et al. (2004).

do represent true liquids without any accumulated crystals. This is the simplest and most straightforward interpretation of the available data. Gusev crater is located in the northernmost region of the highly cratered southern highlands, and olivine-bearing basalts have been documented from spectroscopic measurements elsewhere in the southern highlands (e.g., in the cliffs surrounding Isidis Planitia [Hoefen et al. 2003]), suggesting that this basalt composition may represent an important component of the ancient Martian crust.

We present the results of high-pressure, high-temperature phase equilibrium experiments on the Gusev basalts. The purpose of this study is to understand the formation conditions of these rocks, and we show that these basalts represent the first samples of near-primary magmas from Mars. On Earth, such primary basalts have been extensively used as the main tool to decipher melting conditions and thermal structure of the mantle (BVSP 1981). Similarly, detailed study of the Gusev basalts could give information on mantle composition, mantle processes, and melt generation on the early Mars. Low-pressure crystallization experiments are also used to determine the differentiation path of the Gusev basalts and elucidate their relation to remotely sensed crustal compositions and SNC meteorites.

EXPERIMENTAL METHODS

Starting Materials

The starting composition for this study (Table 1) was a synthetic analog of the average of the published compositions for Adirondack, Humphrey, and Mazatzal (McSween et al. 2006a) based on the recalibrated APXS data (Gellert et al. 2006). An oxide mix was prepared using high-purity oxides (SiO_2, TiO_2, Al_2O_3, Cr_2O_3, Fe_2O_3, MnO, MgO, NiO), synthetic $CaSiO_3$, Na_2SiO_3, and $K_2Si_4O_9$, natural fluorapatite (Durango, Mexico), and Fe sponge (Lindsley et al. 1974). The oxides were ground under ethanol for 5 h in an automatic agate mortar and pestle, then Fe sponge was added and the mixture ground for a final hour.

Low-Pressure Experiments

Equilibrium experiments were performed on the synthetic Gusev basalt analog composition at 0.1 MPa in a Deltech rapid quench gas-mixing furnace. Oxygen fugacity was controlled at or near the quartz-fayalite-magnetite (QFM) buffer using mixtures of CO_2-H_2 gas with volumetric flow rates equal to or less than 0.1 ml/s. Oxygen fugacity was monitored using CaO-ZrO_2 electrolyte cells that were calibrated at the Cu-Cu_2O and Fe-FeO buffers. Temperature was measured using Pt-$Pt_{90}Rh_{10}$ thermocouples calibrated against the melting points of NaCl, Au, and Pd on the IPTS 1968 temperature scale (Biggar 1972).

Forty to fifty mg of the Gusev mix was pressed into a pellet with elvanol as a binder. The pellet was sintered to a FePt alloy loop containing 7–9 wt% Fe designed to minimize the exchange of iron between the silicate charge and the wire loop (Grove 1981). Experimental durations varied from 3 h at near-liquidus conditions to 170 h at the lowest temperatures investigated.

High-Pressure Experiments

Equilibrium experiments were carried out at pressures between 0.8 and 1.5 GPa in a 0.5 inch end-loaded solid medium piston cylinder apparatus (Boyd and England 1960), using the piston-in technique of Johannes et al. (1971). The sample was pressurized to 1.0 GPa (0.8 GPa for 0.8 GPa runs) at room temperature before the temperature was brought up to

865 °C at a rate of 100 °C/min. Temperature was held constant at 865 °C for 6 min and the pressure was raised to the experimental pressure (Table 2). Temperature was then increased to the final experimental temperature at 50 °C/min. Experiments were quenched by turning off the power to the controller. For experiments above 1.0 GPa, the runs were pressure-quenched by reducing pressure to 0.8 GPa as the power was turned off.

About 10 mg of the starting mix was loaded into a graphite crucible with a graphite lid and placed in a platinum capsule that had been triple crimped, welded shut, and flattened on one end. Graphite powder was packed in above and below the crucible (Elkins et al. 2000) and the top of the outer Pt capsule was crimped and welded shut. The capsule was fitted in an alumina sleeve and positioned in the hotspot of a graphite furnace using MgO spacers. $BaCO_3$ cells wrapped with Pb foil were used as the pressure medium. The pressure was calibrated against the reaction anorthite + gehlenite + corundum = Ca-Tschermak (Hays 1966), and is accurate to ±50 MPa. $W_{97}Re_3$-$W_{75}Re_{25}$ thermocouples were used to monitor and control temperature, with no correction for pressure effects on thermocouple EMF. A 20 °C correction was applied to account for the temperature difference between the sample in the hotspot and the location of the thermocouple. This temperature difference was measured by offset thermocouples. The thermal gradient over the length of the sample is less than 10 °C (Wagner and Grove 1997) and the temperature is thought to be accurate to ±10 °C.

The oxygen fugacity (fO_2) imposed by the graphite capsule in our piston cylinder experimental assembly has not been measured directly, although it is expected to lie somewhere between the graphite-CO-CO_2 and the Fe-FeO buffers (Holloway et al. 1992), i.e., between QFM-1.5 and QFM-3.5 under the investigated experimental conditions. Using a nearly identical experimental configuration, Righter and Hauri (1998) determined a fO_2 around FMQ-2.5 using Co-CoO-MgO sensors.

No special effort was made to reduce water adsorption in our "nominally anhydrous" starting material for high-pressure experiments. Similar experiments in our lab have been shown to contain between 0.8 and 1.2 wt% bulk H_2O (Gaetani and Grove 1998; Hauri et al. 2006). The H_2O concentration in experimental glass GUS-20 was determined using the Cameca IMS 3f ion microprobe at Woods Hole Oceanographic Institution, using a series of hydrous basaltic glass standards with H_2O content ranging from 0.05 to 1.00 wt%. Detailed analytical conditions can be found in Sisson and Layne (1993). The average of two analyses is 0.80 ± 0.15 wt% H_2O.

Analytical Methods

The experimental run products were analyzed with the 4- or 5-spectrometer JEOL 733 Superprobe electron microprobes at the Massachusetts Institute of Technology. An accelerating voltage of 15 kV and a beam current of 10 nA were used. Beam size was set to 2 μm for crystalline phases and 10 μm for glasses. Quantitative analyses were obtained using the Armstrong (1995) CITZAF correction package, which uses the Duncumb and Reed atomic number correction, the Reed fluorescence correction, and Heinrich's tabulation of mass-absorption coefficients. To minimize Na loss, the element was counted for 5 s at the beginning of an analysis. Other elements were counted for up to 40 s depending on abundance level. See Gaetani and Grove (1998) for a discussion of analytical precision.

EXPERIMENTAL RESULTS

Approach to Equilibrium

The experiments presented in this study are synthesis experiments where crystals and liquid formed from a starting material that consisted of an oxide mixture. Phase appearance temperatures have not been reversed because previous experience indicates that synthesis experiments are sufficient for determining equilibrium phase appearance temperatures when >40% melt is still present (e.g., Grove and Bence 1977). As demonstrated by Falloon et al. (1999), the use of oxide starting material in high-pressure melting experiments allows a closer approach to equilibrium than the use of crystalline starting materials.

An important prerequisite for the attainment of equilibrium is that the bulk composition of the charge remains constant. Phase proportions in experimental charges were estimated using the least-squares materials balance technique of Bryan et al. (1969) on the compositions of crystals and liquids produced in the experiments (Table 3) to identify the loss or gain of iron. Four piston-cylinder experiments contain only a small amount of spinel crystals (Table 2), and their bulk FeO content is close to the FeO content of the Gusev basalts, indicating no or extremely small Fe loss. The average bulk composition of these experiments has been calculated by mass-balance, and used as an estimate of the starting composition (Table 1). For other experiments, Fe loss or gain was very low, with experimental bulk compositions within 3% relative of the composition of the starting material. The sum of squared residuals (R^2) (Table 2) indicates how well the experimental products represent the starting compositions. A value of 0.0 indicates a perfect fit; all experiments have values below 0.4, indicating that a constant bulk composition has been maintained.

Our estimated starting composition contained somewhat lower Na_2O than the Gusev basalt composition. This difference in Na was not corrected for because we felt that the experimental composition (1.77 wt%) was sufficiently close to that of the APXS analyses, which range from 2.09 to 2.62 (McSween et al. 2006a), and certainly within analytical

Table 2. Experimental conditions and products.

Run no.	Pressure (MPa)	Temp (°C)	Time (h)	Phases[a]	K_D ol/liq	K_D pyx/liq	K_D sp/liq	K_D pl/liq	Mg# gl	Mg# ol	Mg# pyx	Cr# sp	Ca# pl	ΣR^{2} [b]	ΔFe[c]
GUS-35	0.1	1125	170	ol (20) + pig (7) + pl (11) + sp (1) + gl (61)	0.31	0.27	2.13	0.79	0.35	0.64	0.67	0.61	0.70	0.35	2.2
GUS-34	0.1	1145	139	ol (18) + pig (<1) + pl (1) + sp (2) + gl (79)	0.32	–	1.88	0.82	0.40	0.68	–	0.58	0.73	0.39	2.2
GUS-33	0.1	1150	118	ol (18) + sp (2) + gl (80)	0.32	–	2.34	–	0.40	0.68	–	0.53	–	0.41	1.5
GUS-36	0.1	1195	25	ol (12) + sp (2) + gl (86)	0.30	–	1.83	–	0.44	0.72	–	0.61	–	0.38	2.1
GUS-31	0.1	1260	4.5	ol (1) + sp (1) + gl (98)	0.31	–	1.97	–	0.51	0.77	–	0.63	–	0.39	1.3
GUS-32	0.1	1280	4	sp (1) + gl (99)	–	–	1.83	–	0.52	–	–	0.62	–	0.32	0.3
GUS-28	800	1300	4.5	ol (3) + sp (1) + gl (96)	0.34	–	1.60	–	0.50	0.75	–	0.66	–	0.23	0.6
GUS-29	800	1325	4.5	sp (1) + gl (99)	–	–	1.34	–	0.53	–	–	0.67	–	0.34	–2.1
GUS-21	1000	1310	4	ol (3) + opx (<1) + sp (1) + gl (96)	0.35	0.30	1.35	–	0.50	0.74	0.77	0.59	–	0.20	0.8
GUS-20	1000	1330	3	sp (1) + gl (99)	–	–	1.40	–	0.51	–	–	0.63	–	0.23	2.9
GUS-16	1000	1350	2	sp + gl	–	–	–	–	–	–	–	–	–	–	–
GUS-25	1200	1315	3.5	opx (9) + sp (1) + gl (90)	–	0.30	1.34	–	0.47	–	0.75	0.57	–	0.31	–0.1
GUS-24	1200	1335	3.25	sp (1) + gl (99)	–		1.51	–	0.52	–	–	0.64	–	0.27	0.5
GUS-23	1200	1355	2.25	sp + gl	–	–	–	–	–	–	–	–	–	–	–
GUS-17	1200	1375	2.5	sp + gl	–	–	–	–	–	–	–	–	–	–	–
GUS-18	1200	1390	2	sp + gl	–	–	–	–	–	–	–	–	–	–	–
GUS-27	1500	1380	3	sp (1) + gl (99)	–	–	1.36	–	0.52	–	–	0.66	–	0.34	–1.3
GUS-26	1550	1360	3	opx (2) + sp (1) + gl (97)	–	0.31	1.28	–	0.50	–	0.76	0.58	–	0.22	0.9

[a]Abbreviations: gl = glass; ol = olivine; pyx = pyroxene (including opx = orthopyroxene and pig = pigeonite); sp = spinel. Phase proportions calculated by mass balance.
[b]Sum of squared residuals from mass balance calculation.
[c]Apparent loss or gain of FeO estimated as $([FeO_{calculated} - FeO_{starting\ material}]/FeO_{starting\ material})*100$.

Table 3. Electron microprobe analyses of the phases produced in experiments.

Run no.	Phase[a]	SiO_2	TiO_2	Al_2O_3	Cr_2O_3	FeO	MnO	MgO	CaO	Na_2O	K_2O	P_2O_5	NiO	Total[b]
0.1 MPa														
GUS-35	gl (10)[c]	49.9 (4)[d]	0.85 (7)	12.1 (1)	0.10 (7)	18.2 (2)	0.39 (3)	5.60 (20)	10.3 (1)	1.89 (11)	0.15 (1)	0.91 (8)	–	100.38
	ol (5)	36.8 (4)	–	0.07 (5)	0.13 (3)	31.4 (5)	0.61 (6)	30.7 (5)	0.43 (5)	–	–	–	0.05 (1)	100.22
	pig (9)	53.4 (4)	0.12 (3)	1.14 (31)	0.37 (6)	19.3 (1)	0.61 (2)	21.7 (5)	4.39 (3)	0.05 (3)	–	–	–	101.05
	pl (8)	50.8 (5)	–	30.3 (4)	–	1.35 (13)	–	0.29 (6)	14.3 (2)	3.34 (18)	0.03 (1)	–	–	100.39
	sp (8)	0.28 (11)	2.03 (19)	14.6 (1.0)	33.4 (2.0)	40.8 (9)	0.43 (4)	5.91 (12)	0.31 (4)	–	–	–	–	99.3
GUS-34	gl (13)	50.5 (3)	0.65 (7)	13.1 (1)	0.04 (2)	17.2 (2)	0.36 (4)	6.40 (12)	10.1 (1)	1.65 (16)	0.11 (1)	0.65 (5)	–	100.80
	pl (7)	50.6 (8)	–	30.8 (5)	–	1.30 (14)	–	0.35 (7)	14.8 (4)	2.95 (20)	0.03 (1)	–	–	100.70
	ol (6)	36.7 (5)	–	0.09 (3)	0.16 (9)	28.4 (2)	0.55 (4)	33.2 (4)	0.38 (2)	–	–	–	0.10 (2)	99.62
	sp (4)	0.28 (12)	1.04 (1)	18.1 (5)	36.8 (3)	34.5 (3)	0.40 (4)	6.82 (13)	0.30 (3)	–	–	–	–	99.29
GUS-33	gl (11)	50.3 (3)	0.64 (7)	13.2 (7)	0.11 (3)	16.8 (2)	0.40 (2)	6.36 (10)	9.90 (16)	1.52 (11)	0.11 (1)	0.66 (7)	–	99.93
	ol (8)	36.6 (3)	–	0.06 (1)	0.10 (3)	28.1 (2)	0.57 (2)	33.6 (2)	0.31 (3)	–	–	–	0.08 (2)	99.34
	sp (4)	0.32 (3)	1.07 (7)	21.0 (2.1)	34.9 (2.1)	35.2 (5)	0.39 (3)	5.68 (95)	0.23 (9)	–	–	–	–	99.64
GUS-36	gl (11)	49.7 (2)	0.64 (6)	12.1 (1)	0.04 (2)	18.2 (2)	0.40 (3)	7.91 (8)	9.34 (7)	1.53 (12)	0.09 (1)	0.61 (5)	–	100.57
	ol (5)	37.3 (4)	–	0.06 (1)	0.11 (4)	25.5 (3)	0.13 (3)	36.5 (4)	0.35 (3)	–	–	–	0.03 (2)	100.00
	sp (4)	0.49 (25)	0.74 (25)	16.1 (7)	37.3 (1.7)	34.4 (1.1)	0.16 (5)	8.15 (39)	0.25 (5)	–	–	–	–	98.88

Table 3. *Continued.* Electron microprobe analyses of the phases produced in experiments.

GUS-31	gl (10)	47.9 (3)	0.49 (6)	11.0 (1)	0.09 (7)	19.0 (3)	0.42 (4)	10.9 (2)	8.5 (1)	1.28 (7)	0.09 (1)	0.56 (4)	–	100.20
	ol (7)	38.0 (3)	–	0.06 (1)	0.12 (4)	21.4 (5)	0.41 (2)	39.3 (4)	0.26 (1)	–	–	–	0.11 (3)	99.70
	sp (5)	0.31 (17)	0.65 (5)	16.5 (4)	42.5 (4)	29.5 (3)	0.38 (4)	8.6 (8)	0.25 (5)	–	–	–	–	99.68
GUS-32	gl (10)	47.5 (2)	0.49 (10)	10.94 (4)	0.17 (2)	18.9 (2)	0.40 (4)	11.6 (2)	8.20 (10)	1.51 (9)	0.09 (1)	0.62 (1)	–	100.36
	sp (3)	0.33 (14)	0.57 (3)	16.2 (6)	43.2 (1.0)	28.7 (4)	0.35 (4)	9.99 (20)	0.30 (2)	–	–	–	–	100.64
0.8 GPa														
GUS-28	gl (10)	47.1 (3)	0.51 (7)	10.9 (2)	0.22 (7)	18.7 (3)	0.47 (6)	10.4 (2)	8.39 (8)	1.83 (14)	0.06 (1)	0.58 (12)	99.08	–
	ol (5)	37.7 (5)	–	0.06 (1)	0.22 (2)	22.8 (5)	0.42 (2)	37.5 (2)	0.25 (2)	–	–	–	0.02 (2)	99.00
	sp (3)	0.68 (10)	0.48 (2)	17.0 (3)	48.7 (3)	24.2 (1)	0.37 (4)	8.41 (47)	0.15 (7)	–	–	–	–	100.23
GUS-29	gl (10)	47.3 (3)	0.45 (4)	10.7 (1)	0.32 (6)	18.5 (4)	0.41 (3)	11.6 (2)	8.14 (7)	1.86 (13)	0.05 (1)	0.59 (9)	–	99.88
	sp (4)	0.83 (38)	0.44 (2)	16.1 (7)	49.9 (6)	22.1 (2)	0.30 (4)	10.4 (4)	0.30 (10)	–	–	–	–	100.62
1.0 GPa														
GUS-21	gl (11)	46.6 (3)	0.54 (10)	11.0 (1)	0.25 (4)	18.7 (2)	0.44 (4)	10.4 (1)	8.45 (9)	1.93 (13)	0.063 (5)	0.67 (11)	99.13	–
	ol (7)	37.3 (2)	–	0.06 (2)	0.21 (2)	23.6 (2)	0.41 (3)	37.3 (2)	0.28 (2)	–	–	–	0.03 (3)	99.16
	opx (10)	53.6 (2)	0.04 (2)	2.52 (7)	1.09 (5)	14.3 (2)	0.35 (4)	26.6 (3)	1.52 (10)	0.09 (5)	–	–	–	100.09
	sp (4)	1.2 (1)	0.47 (2)	20.5 (1.2)	44.2 (9)	23.3 (6)	0.38 (3)	9.6 (5)	0.33 (6)	–	–	–	–	100.20
GUS-20	gl (13)	46.6 (2)	0.42 (6)	10.5 (1)	0.27 (4)	19.3 (1)	0.44 (3)	11.4 (1)	8.06 (12)	1.82 (14)	0.07 (1)	0.56 (5)	–	99.52
	sp(4)	0.39 (15)	0.41 (1)	18.1 (2)	47.0 (1)	23.3 (3)	0.34 (3)	9.82 (11)	0.21 (2)	–	–	–	–	99.96
1.2 GPa														
GUS-25	gl (10)	46.5 (3)	0.61 (7)	11.5 (1)	0.27 (3)	19.0 (2)	0.42 (5)	9.44 (22)	8.77 (10)	1.86 (20)	0.06 (1)	0.64 (9)	–	99.11
	opx (9)	53.5 (2)	0.07 (1)	3.16 (7)	1.20 (4)	15.2 (4)	0.35 (4)	25.5 (2)	1.73 (8)	0.09 (2)	–	–	–	100.75
	sp (4)	0.64 (23)	0.46 (1)	21.1 (3)	42.2 (5)	24.8 (7)	0.39 (3)	9.20 (34)	0.26 (4)	–	–	–	–	99.33
GUS-24	gl (12)	46.9 (3)	0.53 (4)	10.5 (2)	0.32 (4)	18.8 (3)	0.42 (4)	11.3 (2)	7.96 (10)	1.71 (11)	0.06 (1)	0.54 (6)	–	99.10
	sp (3)	0.47 (7)	0.42 (2)	17.8 (1.5)	47.7 (2)	23.4 (4)	0.36 (3)	9.30 (40)	0.23 (3)	–	–	–	–	99.97
1.5 GPa														
GUS-26	gl (9)	46.7 (2)	0.55 (5)	10.79 (7)	0.34 (3)	18.9 (2)	0.38 (2)	10.69 (9)	8.22 (9)	1.85 (7)	0.06 (1)	0.57 (8)	–	99.11
	opx (10)	53.2 (4)	0.03 (1)	2.85 (45)	1.29 (17)	14.8 (2)	0.08 (2)	26.6 (3)	1.50 (8)	0.09 (2)	–	–	–	100.41
	sp (5)	0.34 (8)	0.38 (2)	20.8 (6)	43.5 (9)	23.8 (4)	0.11 (2)	10.5 (3)	0.17 (2)	–	–	–	–	100.09
GUS-27	gl (11)	47.0 (3)	0.52 (9)	10.5 (1)	0.53 (3)	18.4 (2)	0.42 (4)	11.2 (2)	8.01 (8)	1.70 (10)	0.05 (1)	0.55 (5)	–	99.04
	sp (3)	0.34 (16)	0.36 (3)	17.1 (7)	49.7 (1.6)	22.5 (4)	0.27 (14)	10.1 (5)	0.22 (2)	–	–	–	–	100.84

[a]Abbreviations: gl = glass; ol = olivine; pyx = pyroxene (including opx = orthopyroxene and pig = pigeonite); sp = spinel. Phase proportions calculated by mass balance.

[b]Spinel totals summed using FeO and Fe_2O_3 values reported in Table 4.

[c]Number of microprobe analyses.

[d]One standard deviation of replicate analyses in terms of last unit cited. Thus 49.9 (4) should be read as 49.9 ± 0.4.

Table 4. Fe_2O_3 and FeO estimates in spinels based on charge balance.

Pressure	Run no.	Fe_2O_3	FeO
0.1 MPa	GUS-35	16.1	26.3
	GUS-34	10.9	24.7
	GUS-33	8.9	27.2
	GUS-36	13.2	22.4
	GUS-31	8.9	21.5
	GUS-32	10.1	19.6
0.8 GPa	GUS-28	1.7	22.7
	GUS-29	2.6	19.8
1.0 GPa	GUS-21	1.6	21.9
	GUS-20	3.5	20.1
1.2 GPa	GUS-25	3.5	21.6
	GUS-24	2.7	21.0
1.5 GPa	GUS-26	4.6	19.7
	GUS-27	3.0	19.8

uncertainties for Na by APXS. The small variations in phase relations caused by this difference in Na are thus within the uncertainty on phase relations caused by the inherent uncertainty of the APXS measurements. There was also some unavoidable loss of Na in the 0.1 MPa experiments, despite the low gas flow rates, and these losses come with the need to use long experimental durations to achieve exchange equilibrium between silicate crystals and melt. Tormey et al. (1987) and Grove and Juster (1989) discuss the trade-off in attempting to achieve equilibrium in 0.1 MPa gas-mixing experiments. Crystallization models were constructed to account for the effect of Na loss on the low pressure liquid line of descent.

Approach to equilibrium was evaluated following the criteria devised by Grove and Juster (1989), and is demonstrated by regular major-element partitioning between crystalline phases and liquid. The average mineral-melt Fe-Mg exchange distribution coefficient for olivine ($K_D^{Fe\text{-}Mg}$ olivine = $[X_{Fe}^{ol}X_{Mg}^{liq}]/[X_{Mg}^{ol}X_{Fe}^{liq}]$) is 0.32 ± 0.02 (Table 2; 1 standard deviation), and 0.30 ± 0.01 for orthopyroxene (Table 2). For spinel, the $K_D^{Fe\text{-}Mg}$ for the 0.1 MPa experiments is 2.0 ± 0.2 and for the piston cylinder experiments it is 1.40 ± 0.11. The different values for the spinel $K_D^{Fe\text{-}Mg}$ may relate to differences in ferric iron in the low and high pressure experiments (Table 4). Spinels in the high-pressure experiments have an average of 2.9 wt% Fe_2O_3 based on mineral formula renormalizations, and the spinels in the 0.1 MPa experiments have 11.4 wt% Fe_2O_3. The single 0.1 MPa experiment with pigeonite large enough to analyze has a $K_D^{Fe\text{-}Mg}$ of 0.27. Although we cannot confirm that all elements approached equilibrium, the consistent $K_D^{Fe\text{-}Mg}$ values are an indication that minerals have established Fe-Mg exchange equilibrium with surrounding melt. The average plagioclase-melt Ca-Na exchange distribution coefficient ($K_D^{Ca\text{-}Na}$ plagioclase = $[X_{Ca}^{plag}X_{Na}^{liq}]/[X_{Na}^{plag}X_{Ca}^{liq}]$) for the two 0.1 MPa experiments with plagioclase is 0.80 ± 0.02.

High-Pressure Phase Relations

A pressure-temperature phase diagram for the Gusev basalt composition is presented in Fig. 1 and representative phase compositions are given in Table 3. Cr-rich spinel (Cr# = Cr/[Cr + Al] = 0.5–0.7) (Table 2) is the first phase to crystallize at all pressures investigated. We did not attempt to locate the spinel liquidus because spinel stability is highly dependent on the oxygen fugacity (fO_2) and Cr_2O_3 content of the starting material. In particular, the Cr_2O_3 content of spinel-saturated melts shows a strong increase with decreasing fO_2 near the iron/wüstite (IW) buffer (Roeder and Reynolds 1991). The average Cr_2O_3 in our experimental glasses (0.36 wt%) (Table 1) is consistent with a fO_2 between QFM-2 and QFM-3 (Roeder and Reynolds 1991), which is in good agreement with fO_2 estimates for our experimental assembly (Righter and Hauri 1998). The starting material, which contains 0.78 wt% Cr_2O_3, is oversaturated respective to spinel, and precipitates Cr-rich spinel throughout a wide range of pressure/temperature conditions. If the fO_2 was one log unit lower (FMQ-3.5 = IW), the equilibrium Cr_2O_3 solubility would be 0.50–0.63 wt% at spinel saturation (Roeder and Reynolds 1991). The recalibrated Gusev composition contains 0.63 wt% Cr_2O_3, and is thus expected to be right at spinel saturation for a fO_2 of IW. Estimates from mineralogy of Martian meteorites (e.g., Wadhwa 2001) indeed suggest an oxygen fugacity near IW in the Martian mantle. Our experiments are thus artificially oversaturated in spinel due to higher fO_2, but since crystallization of a small and constant amount of Cr-rich spinel in every experiment does not significantly change the bulk composition (except for chromium, Table 1), it should not have any significant effect on phase relations and could thus be neglected.

At 0.1 MPa, the first silicate to crystallize is olivine (Mg# = molar [Mg/(Mg + Fe)] = 0.77) at 1270 °C. Olivine and spinel co-crystallize until 1145 °C, when plagioclase (An_{73}) and pigeonite join the crystallizing assemblage. At 1145 °C, the charge contains 18 wt% Fo_{68} olivine, with a 21 wt% total crystallinity. Our lowest temperature experiment at 1125 °C contained 20% Fo_{64} olivine, 7% pigeonite, 11% An_{70} plagioclase, and 1% spinel.

At 1.0 GPa and 1320 °C, the Gusev basalt composition is multiply saturated with olivine (Mg# 0.74), orthopyroxene (Mg# 0.77), and chromium-rich spinel. The multiple saturation does not truly occur on the liquidus, since the spinel is stable to much higher temperatures. However, as discussed above, spinel is overstabilized in the experiments, and we consider that Gusev basalts would be saturated on or near their liquidus with olivine, orthopyroxene and spinel for an oxygen fugacity near IW. At pressures above the 1.0 GPa multiple saturation point, orthopyroxene is the first silicate phase to crystallize after spinel. At 1.2 GPa, opx (Mg# 0.75) appears at 1315 °C, and at 1.5 GPa, opx of Mg# 0.76 crystallizes at 1360 °C. Below 1.0 GPa, olivine is the first

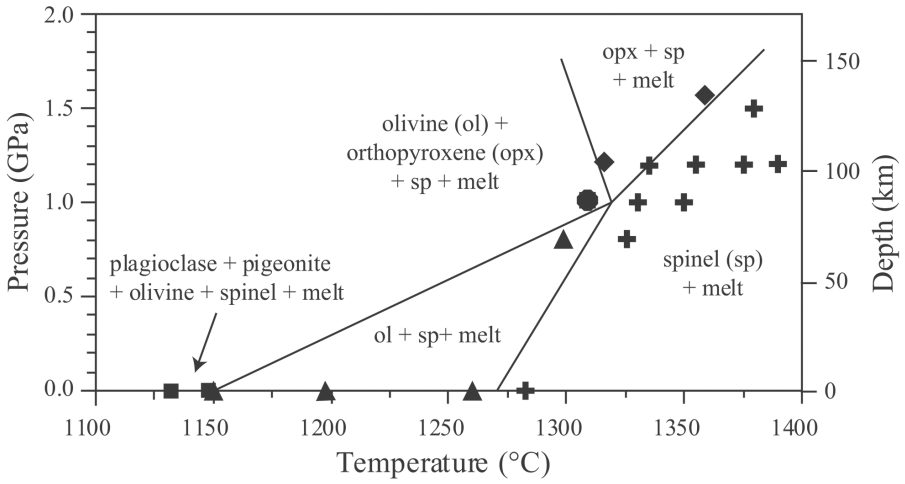

Fig. 1. An experimental phase diagram for the recalibrated Gusev basalt composition. Spinel is the liquidus phase at all investigated pressures, but its stability is highly dependent on oxygen fugacity (Roeder and Reynolds 1991). We thus consider that an olivine + orthopyroxene + spinel multiple saturation point occurs on the liquidus near 1320 °C and 1.0 GPa (85 km depth).

silicate phase to crystallize, and at 0.8 GPa, Fo_{75} olivine appears at 1300 °C.

Monders et al. (2005) carried out an experimental investigation of the Gusev basalt composition initially reported by the Spirit Rover team (McSween et al. 2004) (Table 1). It was later discovered that the sensor heads on the two Mars Rovers had been switched and the calibrations used in APXS data reduction were incorrect. Experimental results for this initial composition are presented in the Appendix and show that the differences in composition between the two analyses result in small but resolvable differences in the conditions of multiple saturation. Compared to the recalibrated composition, the multiple saturation point for the preliminary composition was at 1.1 GPa and 1360 °C, a consequence of the higher MgO in the preliminary composition. The saturating liquidus phases remained the same (olivine + opx + spinel).

The high-pressure experiments contain a small (~0.8 wt%) amount of H_2O, which is well known to have a strong influence on phase relations. The amount of H_2O contained in Gusev basalts is unknown, since if there was water, it likely degassed upon eruption. An experimental study by Pichavant et al. (2002) on primitive subduction zone basalts shows that H_2O decreases the liquidus temperature, but has only a very small effect on multiple saturation pressure. Reasonable H_2O contents for primitive basalts on Earth (i.e., 0–2.5 wt% H_2O) (Sobolev and Chaussidon 1996) would translate in liquidus variations of ±40 °C compared to our experiments (Pichavant et al. 2002), i.e., the multiple saturation temperature would be between 1280 and 1360 °C.

Liquid Line of Descent

Experiments at 0.1 MPa can be used to constrain the low-pressure crystallization path for Gusev basalt. The low-pressure liquid line of descent (Fig. 2) has been calculated using the phase proportions and appearance sequence determined in the 0.1 MPa experiments to obtain a more continuous evolution from the scattered experimental points. Calculation also allows correcting for the Na loss in the 0.1 MPa experiments. The calculated evolution and experimental data have been compared to thermodynamic modeling using the MELTS program (Ghiorso and Sack 1995) in order to test the validity of MELTS calculation for Martian magmatic rocks.

The crystallization model consists of small crystallization steps; for each step, proportions and compositions of crystallizing phases are calculated from the experimental phase proportions and experimental partition coefficients. The following crystallization sequence was used: 1% Cr-rich spinel crystallization followed by 18% crystallization of 98% olivine and 2% spinel. When the MgO concentration in the liquid is down to 6.2 wt% (1145 °C for the 0.1 MPa experiments), the appearance of pigeonite as a crystallizing phase means that the residual liquid has reached the olivine-pigeonite reaction boundary, placing olivine in a peritectic reaction with pyroxene + liquid (Grove and Juster 1989). A small amount of olivine (4%) reacts back with the liquid while crystallizing 52% plagioclase, 51% pigeonite, and 1% spinel (olivine + liquid = plagioclase + pigeonite + spinel). The model was continued to 5.03 wt% MgO, close to the MgO content of our lowest temperature experiment (1125 °C). The model fits the experimental trend very well (Fig. 2), except for TiO_2, Na_2O, and SiO_2. The slight offset in TiO_2 (Fig. 2f) may result from the simplifications in modeling spinel crystallization. The mismatch between the fractionation model and the experimental data for Na_2O and SiO_2 (Figs. 2a and 2e) is a result of the unavoidable sodium loss in the 0.1 MPa experiments, which results in lower Na_2O and higher SiO_2 in the residual liquids. The calculated liquid

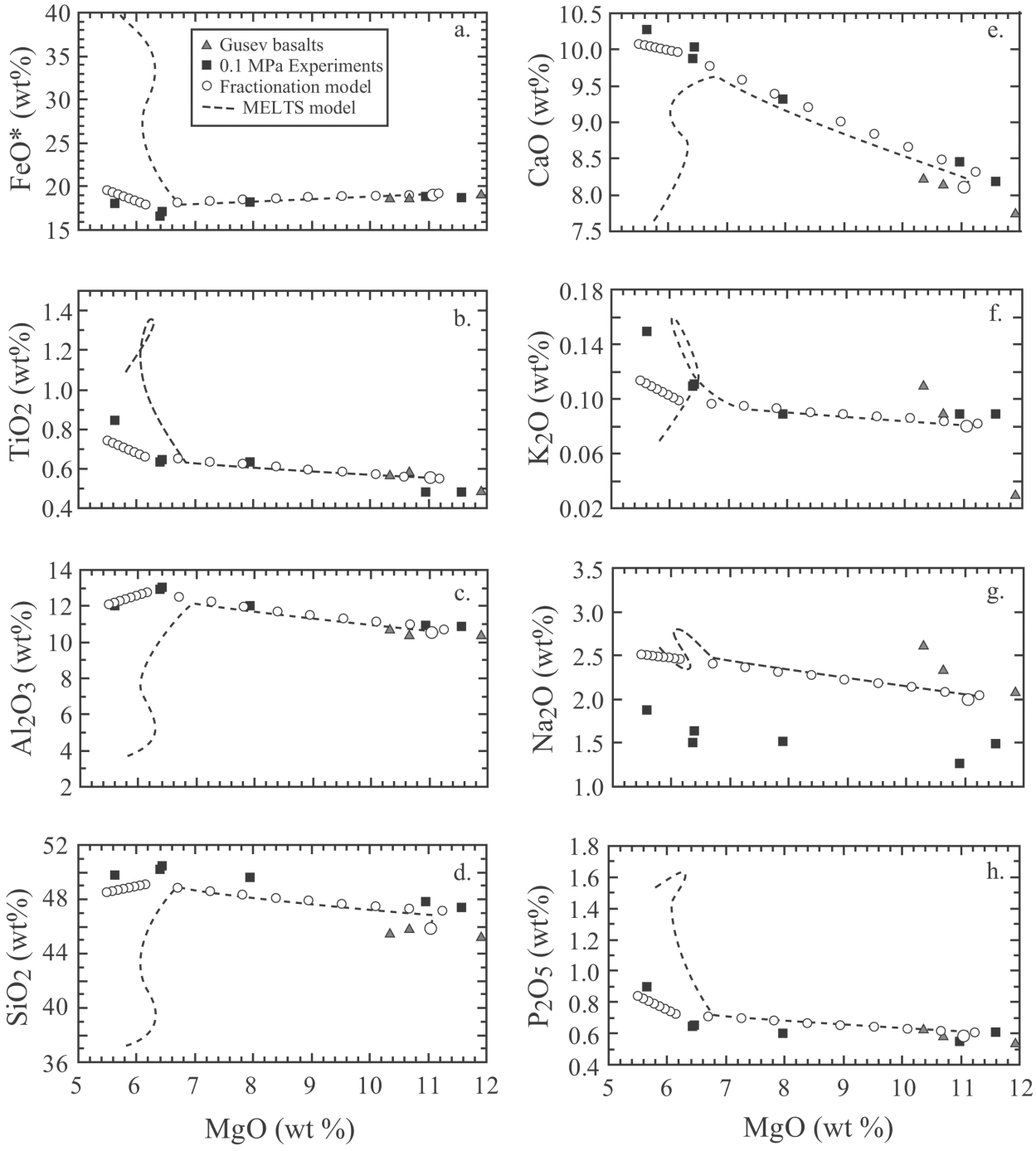

Fig. 2. Low-pressure crystallization path for Gusev basalts: comparison between experimental glasses, our experimentally based crystallization model, and MELTS calculations.

line of descent is thus corrected for the sodium-loss in the experiments, and thus more closely represents the true 0.1 MPa liquid line of descent for Gusev basalts.

Figure 2 and Table 5 compare MELTS (Ghiorso and Sack 1995) calculations with the experimental and model liquid lines of descent for the Gusev composition. Calculations have been performed for temperatures between 1600 and 1090 °C and 0.1 MPa pressure, with oxygen fugacity fixed at the QFM buffer. MELTS recovers the experimental compositions well when spinel and olivine are the only crystallizing phases (Fig. 2). Spinel is present in the highest temperature experiment (1285 °C) and MELTS indicates that it appears at 1535 °C as the liquidus phase. According to melts calculations, olivine Fo_{81} crystallizes at 1275 °C, in lieu of

Fo_{77} olivine in the experiments. Once MELTS reaches 1165 °C (MgO = 6.85 wt%), i.e., when plagioclase and pigeonite appear, the liquid line of descent strongly diverges from the experimental data (Fig. 2). The iron-rich residual liquid produced by this Martian composition are probably in a part of the compositional space that is not well modeled by MELTS, and MELTS should not be used to investigate phase relations and liquid line of descent for Gusev crater basalts and related rocks.

Table 5. Comparison between MELTS calculations and 0.1 MPa experiments (fO_2 = QFM).

Phase appearance	MELTS	Experiments
Spinel	1535 °C	>1280 °C
Olivine	1275 °C	~1270 °C
	Fo_{81}	Fo_{77}
	melt MgO: 10.9	melt MgO: 10.9
Plagioclase	1165 °C	~1145 °C
	An_{67}	An_{73}
	melt MgO: 6.85	melt MgO: 6.40
Pigeonite	1155 °C	~1145 °C
	melt MgO: 6.58	melt MgO: 6.40
Cpx	1130 °C	≤1125 °C
Solidus	1090 °C	≤1125 °C

DISCUSSION

Olivine Megacrysts: Closed System Crystallization or Crystal Accumulation?

There is debate whether the olivine megacrysts observed in Adirondack, Humphrey, and Mazatzal are actual phenocrysts that crystallized in situ or represent an accumulation of crystals by settling in the lower portion of the cooling unit (McSween et al. 2006a). McSween et al. (2004, 2006a) propose that olivine accumulation did not occur and that the basalt composition represents a liquid composition, based on the evidence that the rocks at the Gusev site have similar compositions despite differences in texture and modal olivine. Crystal settling in a lava flow would lead to highly variable rock compositions throughout the flow, depending on cumulate crystal proportions, whereas the three randomly analyzed rocks have very similar composition.

In our experiments, olivine and Cr-rich spinel co-crystallize until about 18 wt% (about 23 vol%) olivine is formed, and then plagioclase and pigeonite join the crystallizing assemblage. Experimental results thus suggest that low-pressure crystallization will lead to early crystallization of about 23 vol% of olivine phenocrysts before crystallization of a pyroxene + plagioclase + olivine groundmass. Point-counting on microscopic images of the least altered of the Gusev basalts (Humphrey) indicates the presence of ~25 vol% olivine megacrysts and pixels counts of grayscale images indicate ~20 vol% olivine megacrysts in a groundmass formed of pyroxene, plagioclase, chromite and phosphates (McSween et al. 2006a), in agreement with experimental results and the idea that olivine crystals in the Gusev basalts are not accumulated by crystal settling or added as xenocrysts. The composition of the olivine crystals at the point where pyroxene and plagioclase join the crystallizing assemblage is Fo_{68}, close to the Fo_{60} suggested by Mössbauer spectroscopy of Gusev basalts (Morris et al. 2004).

Melting Processes in the Martian Mantle

Melting Conditions

In the simple case of batch melting, if a primary basaltic magma segregated from its mantle residue at a given pressure *P* and temperature *T*, it should be multiply saturated on its liquidus with all the residual mantle phases (usually olivine + orthopyroxene ± clinopyroxene ± spinel ± garnet) at *P* and *T*. Furthermore, saturating phases at *P* and *T* should have the same composition than residual mantle phases. Conversely, if a basaltic magma is multiply saturated with mantle phases at one *P*, *T* point on its liquidus, it can be argued to represent a primary mantle magma, and the pressure and temperature of the multiple saturation point would indicate the pressure and temperature of segregation (e.g., BVSP 1981). In the case of pure polybaric fractional melting, multiple saturation points have been suggested to indicate average pressure and temperature of melting (Asimow and Longhi 2004). The Gusev basalt composition is multiply saturated with opx + olivine + spinel near its liquidus at 1.0 GPa and 1320 °C. Opx and olivine near the multiple saturation point (Tables 2 and 3) are enriched in FeO compared to terrestrial mantle minerals (olivine Fo_{74} and opx En_{77}; compare BVSP 1981). However, it is generally agreed that the Martian mantle is enriched in FeO compared to the Earth's mantle (e.g., Dreibus and Wänke 1984; Halliday et al. 2001; Agee and Draper 2004). The experimental results are thus in agreement with Gusev basalt being a primary to near-primary melt of a Martian source region enriched in FeO relative to the Earth's mantle. Average melting conditions are estimated at about 1.0 GPa and 1320 °C.

Source Composition

The composition of the Martian mantle has been estimated by Dreibus and Wänke (1984 and 1985, hereafter referred to as DW), based on the composition of SNC meteorites and cosmochemical constraints. Bertka and Holloway (1994a, 1994b) conducted a series of anhydrous experiments on the DW mantle composition and determined the phase relations from 1.0 to 3.0 GPa and the melt compositions at 1.5 GPa (Figs. 3 and 4). The olivine + opx + spinel multiple saturation point obtained for the Gusev basalts falls very near the olivine + opx + spinel + liquid field determined for the DW primitive Martian mantle composition (Fig. 3). Furthermore, the compositions of olivine and

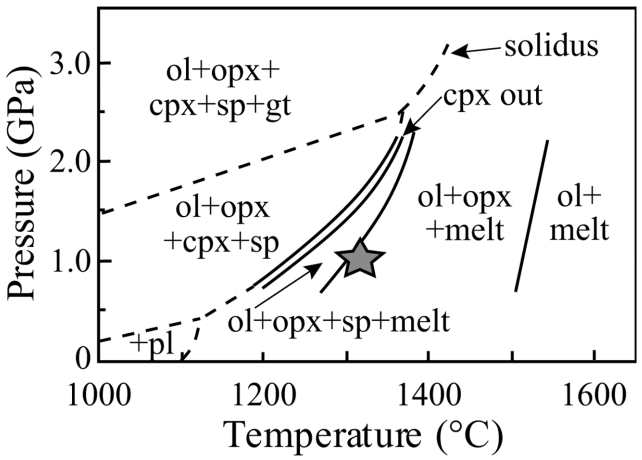

Fig. 3. The Gusev composition (star) is multiply saturated with olivine + opx + spinel at 1.0 GPa and 1320 °C, which is in agreement with the phase diagram for the Dreibus and Wänke (1984) primitive Martian mantle composition (Bertka and Holloway 1994a).

orthopyroxene at the multiple saturation point (Table 2) are similar to the compositions of residual phases from melting experiments on the DW Martian mantle composition (Bertka and Holloway 1994a). This provides additional support to the idea that the melts that formed the Gusev basalts were primary or near-primary magmas from the Martian mantle.

Bertka and Holloway (1994b) did not investigate melt compositions at 1.0 GPa. However, they published a complete data set of melt compositions from the DW Martian mantle at 1.5 GPa. Interestingly, the bulk compositions of Adirondack, Humphrey, and Mazatzal have compositions extremely similar to batch melts of the DW Martian mantle at 1.5 GPa (Fig. 4). In the batch melting hypothesis, basalts multiply saturated at 1.0 GPa should have the same composition as mantle melts at 1.0 GPa, and not mantle melts at 1.5 GPa. However, studies on terrestrial mantle compositions indicate that melt composition only shows a small pressure dependence in the spinel lherzolite stability field (e.g., Kushiro 1996). The similarity between melts of a primitive Martian mantle composition noted above and the Gusev basalts are consistent with derivation of the Gusev magmas from a near-primitive Martian mantle composition. According to Bertka and Holloway's (1994b) experiments, the melt fraction necessary to produce the Gusev basalts would be about 15–20%.

It has been argued that the Dreibus and Wänke (1984) estimate does not represent the composition of the Martian mantle, and other compositions, some very different, have been proposed (e.g., Sanloup et al. 1999; Agee and Draper 2004). In the case of batch melting, saturating phases at the multiple saturation point can be used to constrain the source composition, as a mix of the investigated liquid and the saturating phases, although in unknown proportions. Figure 5 shows the range of potential source compositions for the Gusev basalt. This plot shows that the source has to be strongly enriched in FeO (i.e., lower Mg#) compared to the Earth's mantle. There is no unique solution for the source composition. However, the results presented above make a coherent picture, and key characteristics of the Gusev basalts are in agreement with a DW mantle source. The DW composition has been calculated mainly from cosmochemical data with some constraints from the composition of SNC meteorites. Redoing the same calculation and replacing constraints from SNC meteorites by similar constraints from Gusev basalts composition gives a slightly different mantle composition (DW-Gus) that is, not surprisingly, an even better match for the Gusev basalts mantle source.

Melting Processes

If the Gusev basalts are primary melts of the Martian mantle generated around 1.0 GPa and 1320 °C, what are the consequences on melting processes and crustal evolution on Mars? Two types of melting processes that might have led to the production of the Gusev basalts are batch melting and near-fractional adiabatic decompression melting (Kinzler and Grove 1992). Batch melting would most likely occur during heating of the lithosphere and decompression melting would happen in a convectively ascending mantle melt column; on Earth this process occurs at mid-ocean ridges.

If the Gusev basalts represent batch melts generated around 1.0 GPa (~85 km in depth), an upper limit constraint can be placed on the thickness of the Martian crust and mantle lithosphere in this area at the time of eruption. Age estimates of the Gusev basalt from crater counting are Late Noachian to early Hesperian (3.7 Gyr) (Greeley et al. 2005). Therefore, the early Martian lithosphere beneath the Gusev site would have been thin and mantle conditions would have allowed melting to occur. The current average thickness of the Martian crust near Gusev crater is 50 km (Zuber et al. 2000), and this is likely to have been the crustal thickness in the early Hesperian, since Gusev basalts are the last crust-forming magmatic event in this area. A crustal thickness of 50 km is consistent with a lithosphere 85 km thick (i.e., crust + nonconvecting mantle). The temperature of multiple saturation, 1320 °C, is within the temperature range of Earth's basaltic magmatism (1280–1475 °C) (e.g., Kinzler and Grove 1992; McKenzie and Bickle 1988), indicating that conditions for Martian basalt production would be characterized by high mantle potential temperatures, similar to those on modern Earth. Greeley et al. (2005) suggest that the basalts emplaced on the floor of Gusev crater may be temporally related to volcanic activity on the southern side of Apollinaris Patera and may be the result of regional volcanism around 3.65–3.76 Gyr. This indicates that high mantle potential temperatures, similar to those on modern Earth, persisted on Mars for at least 1.0 Gyr, until the end of the Noachian era.

If melting occurred by near-fractional adiabatic melting, the depth of multiple saturation represents an average depth

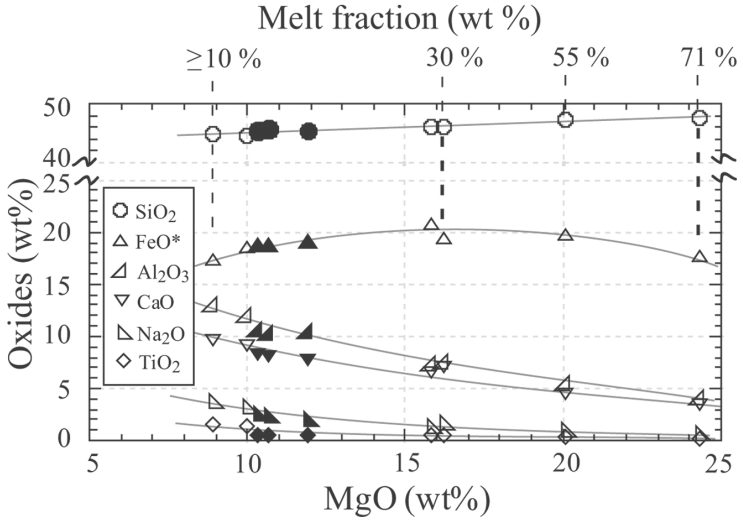

Fig. 4. A comparison between the Gusev basalts (filled symbols) and the 1.5 GPa experimental melting curves (Bertka and Holloway 1994b) of the Dreibus and Wänke (1984) primitive Martian mantle composition (open symbols). The Gusev basalts correspond approximately to a 15–20% melt of a primitive Dreibus and Wänke (1984) Martian mantle.

(or pressure) of melting (Kinzler and Grove 1992). In near-fractional adiabatic decompression melting, small melt increments of melt (~1% melting for 0.1 GPa of upwelling) are produced and continuously separated from the mantle residue. As convecting mantle ascends, it crosses the solidus and begins to melt. At the top of the melting column the fractional melt increments are blended and the resulting aggregate melt represents the average of the melts produced. If the Gusev basalts represent about 15–20% melting of the Martian mantle, and assuming a melt productivity of 10% per 1 GPa (Ahern and Turcotte 1979), the melting interval in the Martian mantle would be 0.75–1 GPa or 64–85 km long melting columns. For a 15% melt with an average depth of generation of 85 km, melting would begin at a depth of 140 km and end at a depth of 20 km. For a 20% melt, melting would begin at a depth of 170 km and end at the surface. Adiabatic near fractional melting would therefore require a very thin lithosphere in the vicinity of melt production of the Gusev basalts, which does not agree with the presence of a crust 50 km thick. Moreover, compositional features preserved in the major elements of modern ocean floor basalts (especially Na_2O and FeO abundances) allow fractional versus batch melting to be distinguished (Kinzler and Grove 1992). For an equivalent extent of melting, fractional melts would be higher in Na_2O and FeO than batch melts. The close correspondence between the Na_2O and FeO content of the DW melts (Fig. 4) and the Gusev basalts is consistent with a batch melting origin.

Possible scenarios for batch melting that seem compatible with the geological evolution of Mars include: 1) generation above a mantle plume related to the Elysium volcanic area, and 2) generation early in Mars' history, when the planet was not yet cooled from early accretionary and impact processing heating and decay of short-lived radiogenic isotopes. From the strong source contrasts with SNC meteorites (see the Reconciling Source Constraints for Gusev Basalts and SNC meteorites section below), which are supposed to come from the young Tharsis and Elysium areas, we believe the first option is less probable. In the second case, Gusev basalts would be part of a primitive Martian basaltic crust.

Relation between Gusev Basalts and the Primitive Martian Crust

Recent investigations by the Spirit Rover have shown a wide magmatic diversity inside Gusev crater. Relatively unaltered rocks on the flank of the Columbia Hills have more evolved compositions than Gusev basalts and may have been formed by fractional crystallization from parental magmas similar to Gusev basalts (McSween et al. 2006b). If rocks near the Spirit landing site can be derived from Gusev-basalt-like parent magmas, could this be generalized to other parts of the Martian crust?

Spectroscopic measurements have shown that most of the southern highlands are covered by rocks of broadly basaltic composition (e.g., Christensen et al. 2000). Olivine has been identified by visible/near-infrared reflectance spectrometry (OMEGA investigation on board the Mars Express spacecraft) (Bibring et al. 2005; Mustard et al. 2005) and thermal emission spectrometry (TES on board the Mars Global Surveyor spacecraft) (Hoefen et al. 2003; Hamilton and Christensen 2005). It is thus possible that olivine basalts similar to the Gusev basalts are representative of at least part of the Noachian southern highlands crust, an idea reinforced by their sampling a relatively primitive mantle source. If this

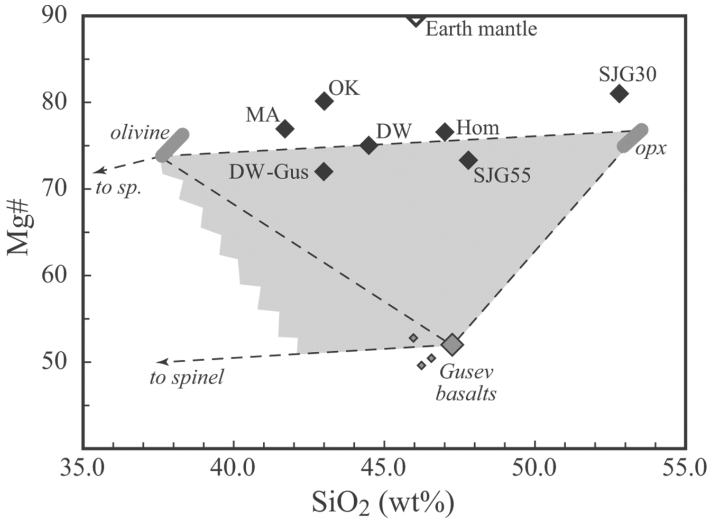

Fig. 5. An estimation of the composition of the source of the Gusev basalts. If Gusev basalts are batch melts, then the composition of their source can be calculated as a mix between residual mantle phases (= multiply saturating phases) and the Gusev basalt composition (gray area). The source has to be strongly enriched in FeO (i.e., lower Mg#) compared to the Earth's mantle (Hart and Zindler 1986). Estimates of the composition of the Martian mantle after Morgan and Anders (1979; MA), Dreibus and Wänke (1984; DW), Ohtani and Kamaya (1992; OK), Sanloup et al. (1999; SJG30, SJG55), and Agee and Draper (2003; Hom). DW-Gus has been calculated following exactly the same process as Dreibus and Wänke (1984), and replacing constraints from SNC meteorites by similar constraints from Gusev basalts.

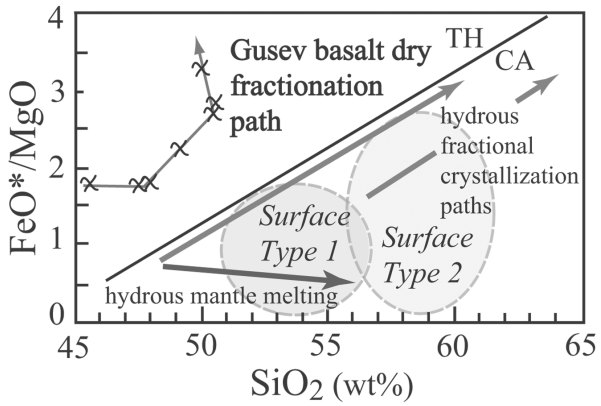

Fig. 6. Low-pressure experiments (X) on the recalibrated Gusev composition show that Gusev basalts follow a tholeiitic (TH) fractionation path and will not produce liquids with a calc-alkaline (CA) surface type 1 or surface type 2 composition under dry conditions. Diagram modified from McSween et al. (2003).

is the case, the parameters derived from the Gusev basalts (lithospheric thickness, mantle temperature, melt fraction) can be used in geophysical models of the formation of the Noachian crust. There are, however, a few caveats. First of all, Gusev basalts are believed to be late Noachian/early Hesperian in age (Greeley et al. 2005), whereas the majority of the Martian crust formed during early Noachian (Nimmo and Tanaka 2005). Nevertheless, similar basalts are likely to have been erupted as long as the same thermal regime prevails, maybe during the first billion years of Martian history. Gusev basalts, located on top of the Martian crust, would record the last event of a hot early Mars.

Also, experimental liquids obtained by low-pressure crystallization of the Gusev basalt composition follow a tholeiitic differentiation trend (Fig. 6) similar to that observed in Iceland or the Galapagos Spreading Center (Juster et al. 1989). The liquid line of descent is characterized by a strong enrichment in FeO with little variation in the SiO_2 content (Fig. 6). Silica-rich rocks are difficult to obtain from such differentiation trends and require a very high degree of crystallization (e.g., Juster et al. 1989). When compared to spectroscopically determined compositions of the Martian surface (surface types 1 and 2) (McSween et al. 2003), differentiation products of Gusev basalts at low pressure have lower silica contents and higher FeO contents; differentiation does not lead toward the compositional field of surface types 1 or 2. There are three ways of reconciling these data: 1) the surface composition is unrelated to Gusev basalts; 2) the Martian crust has been generated under hydrous conditions, since adding water changes the liquid lines of descent from tholeiitic to calcalkaline, producing silica-enriched differentiates (Fig. 6); or 3) most of the early Martian crust has been enriched in silica through alteration (e.g., McSween et al. 2003), and the spectral estimates of the Martian surface does not reflect the original igneous composition.

Reconciling Source Constraints for Gusev Basalts and SNC Meteorites

Apart from the Gusev basalts, olivine-phyric shergottites (e.g., Goodrich 2002; Greshake et al. 2004) are the only known primitive basaltic rocks from Mars. When compared to olivine-phyric shergottites, the Gusev basalts are enriched

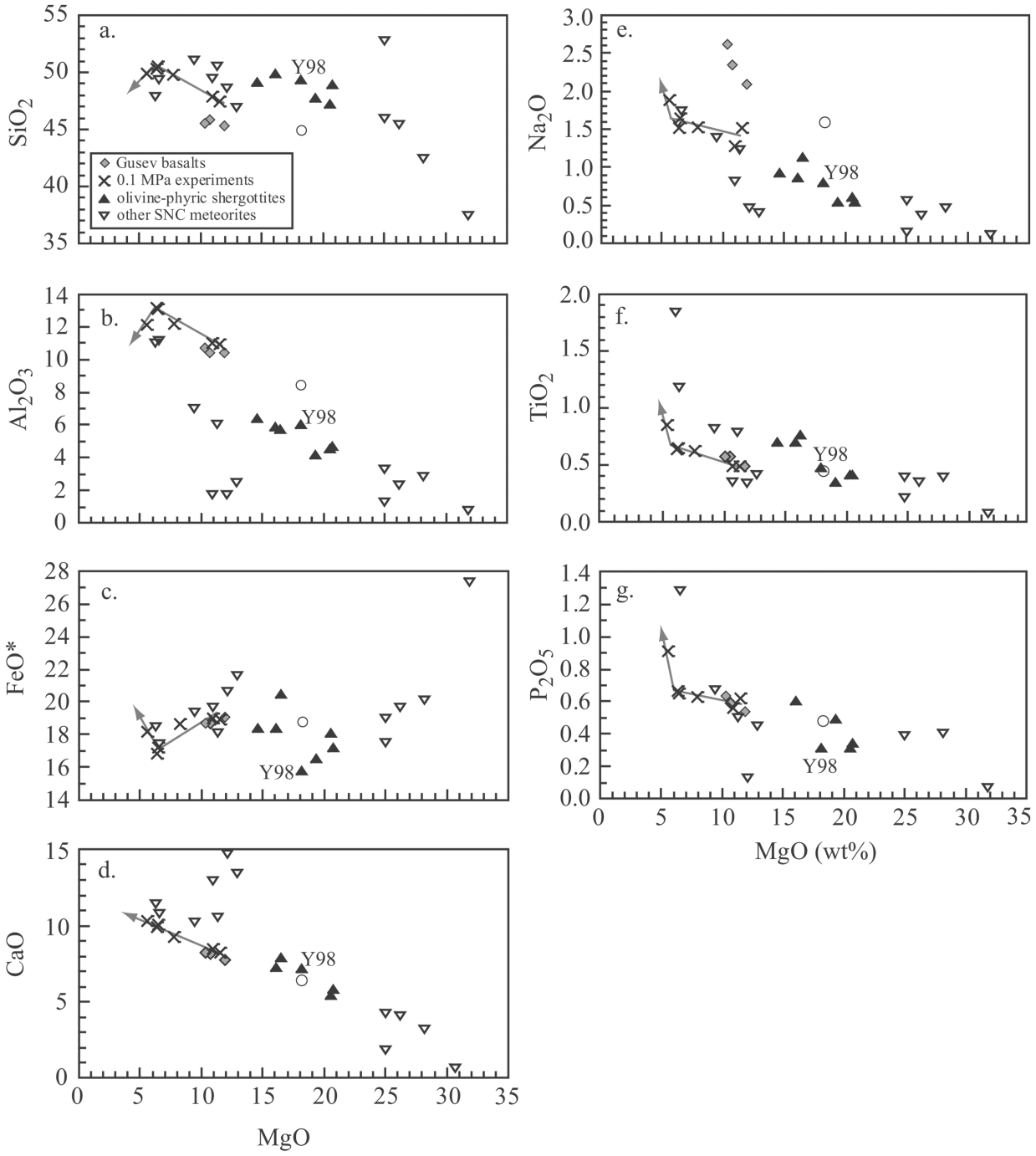

Fig. 7. A comparison between Gusev basalts and SNC meteorites. Low-pressure crystallization (arrow) of the Gusev composition does not produce residual liquids similar to olivine-phyric shergottites or other SNC meteorites. The olivine-phyric shergottite Yamato-980459 (Greshake et al. 2004) is identified on the figure as Y98. The empty circle indicates the effect of adding back equilibrium proportions of olivine and spinel to the Gusev bulk composition to a final MgO content equal to that of Yamato-980459.

in Al_2O_3 and Na_2O (Fig. 7), and have lower CaO/Al_2O_3 ratios (~0.7 compared to 1.1–1.9 for shergottites) (Lodders 1998). Olivine-phyric shergottites are also characterized by higher MgO contents (up to 21 wt%) (Fig. 7) and higher X_{Mg} (~0.66 for olivine-phyric shergottites and ~0.50 for Gusev basalts). Although the similarities of Gusev basalts and olivine-phyric shergottites have been emphasized by some authors (e.g., McSween et al. 2006a), experimental results do not support such comparisons. Low-pressure crystallization of the Gusev basalts slightly modifies the Al_2O_3 content, but the residual liquids still do not evolve to the compositions of any of the olivine-phyric shergottites or other SNC meteorites (Fig. 7).

The olivine-phyric shergottite Yamato-980459 (Y98) (Greshake et al. 2004), which contains the most magnesian olivines (Fo_{84}) of the Martian meteorites, is a good candidate for a primary mantle magma. Experimental work on Y98 shows that it is multiply saturated with olivine and orthopyroxene, with a multiple saturation pressure slightly higher than for the Gusev basalts (~1.2 GPa) and a higher temperature (1550 °C) (Musselwhite et al. 2006). The possibility that Gusev basalts could have been derived from primitive olivine-phyric shergottites through olivine and spinel crystallization has been tested by calculating the effect on the Gusev bulk composition of adding back equilibrium proportions of olivine and spinel in 1% increments. Equilibrium proportions were determined from the 0.1 MPa experimental data. This calculation was carried out to a final MgO content equal to that of Y98 (18.1 wt%) and is shown in Fig. 7. SiO_2, FeO, and Al_2O_3 all have significant discrepancies between the modeled value and the actual oxide value for Y98. The experimental results thus indicate that shergottites cannot be related to the Gusev basalts by simple fractional crystallization, suggesting a different mantle source and/or different genetic processes.

Compared to the source of Gusev basalts, the mantle source for Y98 (and other shergottites) needs to have a higher Mg# (i.e., less FeO) (Fig. 7c) (Agee and Draper 2003) and/or a higher CaO/Al_2O_3 ratio (i.e., less Al_2O_3) (Fig. 7b) (Borg and Draper 2003). Even if most Martian meteorites are relatively young (165–875 Myr for shergottites) (Jones 1986; Nyquist et al. 2001), their source(s) formed very early in Mars history (e.g., Borg et al. 1997; Foley et al. 2005), and the source region for shergottites was already present at the time of Gusev basalts eruption. Is it possible for two really different reservoirs to coexist in the early Martian mantle?

The superchondritic (>1.0, the value observed in chondrites meteorites) CaO/Al_2O_3 ratio of the shergottite mantle source has been argued to originate from garnet fractionation crystallization during an early magma ocean stage (Borg and Draper 2003; Elkins-Tanton et al. 2003). If a planet-wide magma ocean underwent fractional crystallization, the existence of a relatively unmodified primitive source (i.e., similar to the bulk composition of the Martian mantle) for the Gusev basalts seems unlikely at first. However, according to Elkins-Tanton et al. (2003, 2005), fractional crystallization of a magma ocean with a chondritic CaO/Al_2O_3 ratio (~1.0) could result in a deep layer of majorite and ringwoodite with the same chondritic CaO/Al_2O_3 ratio, a small intermediate layer of accumulated garnet ($CaO/Al_2O_3 < 1.0$), and an upper layer of olivine + pyroxenes with a superchondritic CaO/Al_2O_3 ratio (>1.0), due to the extraction of garnet. Subsequent overturn due to gravitational instability would bring together in the upper mantle the deep, mostly unmodified, layer with a chondritic CaO/Al_2O_3 ratio (majorite and ringwoodite will transform to olivine and pyroxenes upon decompression), and the shallow layer with a superchondritic CaO/Al_2O_3 ratio, and also a higher Mg# (Elkins-Tanton et al. 2005). It is thus relatively easy to get two different sources with different CaO/Al_2O_3 ratios in the Martian mantle. This hypothesis works even better in the case of a partial magma ocean. If the energy from accretion, core formation, and radioactivity was too low to melt the entire planet, the deepest layers would be unmodified during magma ocean crystallization. Upper layers would still undergo garnet extraction and have a superchondritic CaO/Al_2O_3 ratio. Mantle overturn due to gravitational instabilities would then bring the deep primitive layers to the upper mantle. Another possibility is that Mars never melted to form a magma ocean, or that the magma ocean evolved through equilibrium crystallization, so that the entire Martian mantle still has a primitive composition similar to the reservoir for Gusev basalts. This hypothesis, however, requires finding a way for generating localized early mantle heterogeneities that would serve as the sources for shergottites.

Finally, widespread aqueous alteration has been observed at Gusev crater, and the source problem between Gusev basalts and shergottite meteorites could be explained if Gusev basalts were modified by weathering, and thus do not represent primitive mantle melts. However, this hypothesis seems highly unlikely, since Gusev basalts contain abundant olivine, a mineral that is easily altered on Earth. Furthermore, alteration trends recorded in the surface layers of Gusev basalts, through successive analyses of dusty, brushed, and ground rocks (McSween et al. 2006a) show similar decreases in CaO and Al_2O_3, and thus almost constant CaO/Al_2O_3 ratios.

CONCLUSIONS

Our experimental work suggests that the Gusev basalts are high-temperature, near-primary shallow melts of a primitive Martian mantle reservoir with a composition similar to the Dreibus and Wänke (1984) estimate. Crater counts indicate that they formed at about 3.6 Gyr, indicating that high mantle potential temperatures, similar to those on modern Earth, persisted for at least a billion years during Martian history. Olivine-rich basalts have been identified throughout the southern highlands and may be related to Gusev basalts, which would then represent an important component of the primitive Martian crust.

The relatively undifferentiated mantle source for the Gusev basalts coexisted with the highly depleted shergottite source throughout Mars history. This reinforces the idea of the absence of global mantle convection and mixing on Mars, and would require that at least part of the mantle stayed relatively primitive during early planetary differentiation.

Acknowledgments–The authors thank Dave Draper, Hanna Nekvasil, and Associate Editor Kevin Righter for their thoughtful reviews. Their comments were very helpful in

revising the paper. This research was supported by a NASA grant MFRP03-0063-0050 and by a National Science Foundation Graduate Research Fellowship.

Editorial Handling—Dr. Kevin Righter

REFERENCES

Agee C. B. and Draper D. S. 2004. Experimental constraints on the origins of the Martian mantle. *Earth and Planetary Science Letters* 224:415–429.

Ahern J. L. and Turcotte D. L. 1979. Magma migration beneath an ocean ridge. *Earth and Planetary Science Letters* 45:115–122.

Armstrong J. T. 1995. CITZAF—A package of correction programs for the quantitative electron microbeam X-ray analysis of thick polished materials, thin films, and particles. *Microbeam Analysis* 4:177–200.

Asimow P. D. and Longhi J. 2004. The significance of multiple saturation points in the context of polybaric near-fractional melting. *Journal of Petrology* 45:2349–2367.

Bertka C. M. and Holloway J. R. 1994a. Anhydrous partial melting of an iron-rich mantle I: Subsolidus phase assemblages and partial melting phase relations at 10 to 30 kbar. *Contributions to Mineralogy and Petrology* 115:313–322.

Bertka C. M. and Holloway J. R. 1994b. Anhydrous partial melting of an iron-rich mantle II: Primary melt compositions at 15 kbar. *Contributions to Mineralogy and Petrology* 115:323–338.

Bibring J.-P., Langevin Y., Gendrin A., Gondet B., Poulet F., Berthé M., Soufflot A., Arvidson R., Mangold N., Mustard J., Drossart P., Stéphane E., Forni O., Gendrin A., Combes M., Drossart P., Encrenaz T., Fouchet T., Merchiorri R., Belluci G., Altieri F., Formisano V., Bonello G., Capaccioni F., Cerroni P., Coradini A., Fonti S., Kottsov V., Ignatiev N., Moroz V., Titov D., Zasova L., Douté S., Schmitt B., Sotin C., Hauber E., Hoffmann H., Jaumann R., Keller U., Arvidson R., Duxbury T., and Forget F. 2005. Mars surface diversity as revealed by the OMEGA/Mars Express observations. *Science* 307:1576–1581.

Biggar G. M. 1972. Diopside lithium metasilicate and the 1968 temperature scale. *Mineralogical Magazine* 38:768–770.

Borg L. E., Nyquist L. E., Taylor L. A., Wiesmann H., and Shih C.-Y. 1997. Constraints on Martian differentiation processes form Rb-Sr and Sm-Nd isotopic analyses of the basaltic shergottite QUE 94201. *Geochimica et Cosmochimica Acta* 61:4915–4931.

Borg L. E. and Draper D. S. 2003. A petrogenetic model for the origin and compositional variation of the Martian basaltic meteorites. *Meteoritics & Planetary Science* 38:1713–1731.

Boyd F. R. and England J. L. 1960. Apparatus for phase equilibrium studies at pressures up to 50 kilobars and temperatures up to 1750 °C. *Journal of Geophysical Research* 65:741–748.

Bryan W. B., Finger L. W., and Chayes F. 1969. Estimating proportions in petrographic mixing equations by least-squares approximation. *Science* 163:926–927.

Basaltic Volcanism Study Project. 1981. *Basaltic volcanism on the terrestrial planets.* New York: Pergamon Press. 1286 p.

Christensen P. R., Bandfield J. L., Smith M. D., Hamilton V. E., and Clark R. N. 2000. Identification of a basaltic component on the Martian surface from thermal emission spectrometer data. *Journal of Geophysical Research* 105:9609–9621.

Dreibus G. and Wänke H. 1984. Accretion of the Earth and the inner planets. In *Proceedings of the 27th International Geological Congress.* Utrecht, The Netherlands: VNU Science Press. pp. 1–20.

Dreibus G. and Wänke H. 1985. Mars, a volatile-rich planet. *Meteoritics* 20:367–381.

Elkins L. T., Fernandes V. A., Delano J. W., and Grove T. L. 2000. Origin of lunar ultramafic green glasses: Constraints from phase equilibrium studies. *Geochimica et Cosmochimica Acta* 54: 2565–2574.

Elkins-Tanton L. T., Parmentier E. M., and Hess P. C. 2003. Magma ocean fractional crystallization and cumulate overturn in terrestrial planets: Implications for Mars. *Meteoritics & Planetary Science* 38:1753–1771.

Elkins-Tanton L. T., Hess P. C., and Parmentier E. M. 2005. Possible formation of ancient crust on Mars through magma ocean processes. *Journal of Geophysical Research* 110, doi:10.1029/2005JE002480.

Falloon T. J., Green D. H., Danyushevsky L. V., and Faul U. H. 1999. Peridotite melting at 1.0 and 1.5 GPa: An experimental evaluation of techniques using diamond aggregates and mineral mixes for determination of near-solidus melts. *Journal of Petrology* 40:1343–1375.

Foley C. N., Wadhwa M., Borg L. E., Janney P. E., Hines R., and Grove T. L. 2005. The early differentiation history of Mars from ^{182}W-^{142}Nd isotope systematics in the SNC meteorites. *Geochimica et Cosmochimica Acta* 69:4557–4571.

Gaetani G. A. and Grove T. L. 1998. The influence of water on melting of mantle peridotite. *Contributions to Mineralogy and Petrology* 131:323–346.

Gellert R., Rieder R., Brückner J., Clark B. C., Dreibus G., Klingelhöfer G., Lugmair G., Ming D. W., Wänke H., Yen A., Zipfel J., and Squyres S. W. 2006. Alpha Particle X-ray Spectrometer (APXS): Results from Gusev crater and calibration report. *Journal of Geophysical Research* 111, doi:10.1029/2005JE002555.

Ghiorso M. S. and Sack R. O. 1995. Chemical mass transfer in magmatic processes IV. A revised and internally consistent thermodynamic model for the interpolation and extrapolation of liquid-solid equilibria in magmatic systems at elevated temperatures and pressures. *Contributions to Mineralogy and Petrology* 119:197–212.

Goodrich C. A. 2002. Olivine-phyric Martian basalts: A new type of shergottite. *Meteoritics & Planetary Science* 37:B31–B34.

Greeley R., Foing B. H., McSween H. Y., Jr., Neukum G., Pinet P., Van Kan M., Werner S. C., Williams D. A., and Zegers T. E. 2005. Fluid lava flows in Gusev crater, Mars. *Journal of Geophysical Research* 110, doi:10.1029/2005JE002401.

Greshake A., Fritz J., and Stöffler D. 2004. Petrology and shock metamorphism of the olivine-phyric shergottite Yamato 980459: Evidence for a two-stage cooling and a single-stage ejection history. *Geochimica et Cosmochimica Acta* 68:2359–2377.

Grove T. L. 1981. Use of FePt alloys to eliminate the iron loss problem in 1-atmosphere gas mixing experiments: theoretical and practical considerations. *Contributions to Mineralogy and Petrology* 78:298–304.

Grove T. L. and Bence A. E. 1977. Experimental study of pyroxene-liquid interaction in quartz-normative basalt 15597. Proceedings, 8th Lunar Science Conference. pp. 1549–1579.

Grove T. L. and Juster T. W. 1989. Experimental investigations of low-Ca pyroxene stability and olivine-pyroxene-liquid equilibria at 1-atm in natural basaltic and andesitic liquids. *Contributions to Mineralogy and Petrology* 103:287–305.

Halliday A. N., Wänke H., Birck J.-L., and Clayton R. N. 2001. The accretion, composition and early differentiation of Mars. *Space Science Reviews* 96:197–230.

Hamilton V. E. and Christensen P. R. 2005. Evidence for extensive olivine-rich bedrock on Mars. *Geology* 33:433–436.

Hart S. R. and Zindler A. 1986. In search of a bulk-Earth composition. *Chemical Geology* 57:247–267.

Hauri E. H., Gaetani G. A., and Green T. H. 2006. Partitioning of

water during melting of the Earth's upper mantle at H_2O-undersaturated conditions. *Earth and Planetary Science Letters* 248:715–734.

Hays J. F. 1966. Lime-alumina-silica. *Carnegie Institution of Washington Yearbook* 65:234–236.

Hoefen T. M., Clark R. N., Bandfield J. L., Smith M. D., Pearl J. C., and Christensen P. R. 2003. Discovery of olivine in the Nili Fossae region of Mars. *Science* 302:627–630.

Holloway J. R., Pan V., and Gudmundsson G. 1992. High-pressure fluid-absent melting experiments in the presence of graphite: oxygen fugacity, ferric/ferrous ratio and dissolved CO_2. *European Journal of Mineralogy* 4:105–114.

Johannes W., Chipman D. W., Hays J. F., Bell P. M., Mao H. K., Newton R. C., Boettcher A. L., and Seifert F. 1971. An interlaboratory comparison of piston cylinder pressure calibration using the albite-breakdown reaction. *Contributions to Mineralogy and Petrology* 32:24–38.

Jones J. J. 1986. A discussion of isotopic systematics and mineral zoning in the shergottites: Evidence for a 180 m.y. igneous crystallization age. *Geochimica et Cosmochimica Acta* 50:969–977.

Juster T. C., Grove T. L., and Perfit M. R. 1989. Experimental constraints on the generation of FeTi basalts, andesites, and rhyodacites at the Galapagos spreading center, 85°W and 95°W. *Journal of Geophysical Research* 94:9251–9274.

Kinzler R. J. and Grove T. L. 1992. Primary magmas of mid-ocean ridge basalts 2. Applications. *Journal of Geophysical Research* 97:6907–6926.

Kushiro I. 1996. Partial melting of a fertile mantle peridotite at high pressures: An experimental study using aggregates of diamond. In *Earth processes: Reading the isotopic code,* edited by Basu A. and Hart S. Washington, D.C.: American Geophysical Union. pp. 109–122.

Lindsley D. H., Kesson S. E., Hartzman M. J., and Cushman M. K. 1974. The stability of armalcolite: Experimental studies in the system Mg-Fe-Ti-O. Proceedings, 5th Lunar Science Conference. pp. 521–534.

Lodders K. 1998. A survey of shergottite, nakhlite, and chassigny meteorites whole-rock compositions. *Meteoritics & Planetary Science* 33:A183–A190.

McKenzie D. and Bickle M. J. 1988. The volume and composition of melt generated by extension of the lithosphere. *Journal of Petrology* 29:625–679.

McSween H. Y., Jr. 1994. What we have learned about Mars from SNC meteorites. *Meteoritics* 29:757–779.

McSween H. Y., Jr. 2002. The rocks on Mars, from far and near. *Meteoritics & Planetary Science* 37:7–25.

McSween H. Y., Jr., Grove T. L., and Wyatt M. B. 2003. Constraints on the composition and petrogenesis of the Martian crust. *Journal of Geophysical Research* 108, doi:10.1029/2003JE002175.

McSween, H. Y. Jr., Arvidson R. E., Bell J. F., Blaney D., Cabrol N. A., Christensen P. R., Clark B. C., Crisp J. A., Crumpler L. S., des Marais D. J., Farmer J. D., Gellert R., Ghosh A., Gorevan S., Graff T., Grant J., Haskin L. A., Herkenhoff K. E., Johnson J. R., Jolliff B. L., Klingelhoefer G., Knudson A. T., McLennan S., Milam K. A., Moersch J. E., Morris R. V., Rieder R., Ruff S. W., de Souza P. A., Squyres S. W., Wänke H.; Wang A., Wyatt M. B., Yen A., and Zipfel J. 2004. Basaltic rocks analyzed by the Spirit Rover in Gusev crater. *Science* 305:842–845.

McSween H. Y., Jr., Wyatt M. B., Gellert R., Bell J. F., Morris R. V., Herkenhoff K. E., Crumpler L. S., Milam K. A., Stockstill K. R., Tornabene L. L., Arvidson R. E., Bartlett P., Blaney D., Cabrol N. A., Christensen P. R., Clark B. C., Crisp J. A., des Marais D. J., Economou T., Farmer J. D., Farrand W., Ghosh A., Golombek M., Gorevan S., Greeley R., Hamilton V. E., Johnson J. R., Joliff B. L., Klingelhöfer G., Knudson A. T., McLennan S., Ming D., Moersch J. E., Rieder R., Ruff S. W., Schröder C., de Souza P. A., Squyres S. W., Wänke H., Wang A., Yen A., and Zipfel J. 2006a. Characterization and petrologic interpretation of olivine-rich basalts at Gusev crater, Mars. *Journal of Geophysical Research* 111, doi:10.1029/2005JE002477.

McSween H. Y., Jr., Ruff S. W., Morris R. V., Bell J. F. III, Herkenhoff K., Gellert R., Stockstill K. R., Ronabene L. L., Squyres S. W., Crisp J. A., Christensen P. R., McCoy T. J., Mittlefehldt D. W., and Schmidt M. 2006b. Alkaline volcanic rocks from the Columbia Hills, Gusev crater, Mars. *Journal of Geophysical Research*, 111, doi:10.1029/2006JE002698.

Middlefehldt D. W. 1994. ALHA84001, a cumulate orthopyroxenite member of the Martian meteorite clan. *Meteoritics* 29:214–221.

Minitti M. M. and Rutherford M. J. 2000. Genesis of the Mars Pathfinder "sulfur-free" rock from SNC parental liquids. *Geochimica et Cosmochimica Acta* 64:2535–2547.

Monders A. G., Médard E., and Grove T. L. 2005. Primary Martian basalts at Gusev crater: Experimental constraints (abstract #2069). 36th Lunar and Planetary Science Conference. CD-ROM.

Morgan J. W. and Anders E. 1979. Chemical composition of Mars. *Geochimica et Cosmochimica Acta* 43:1601–1610.

Morris R. V., Klingelhöfer G., Bernhardt B., Schröder C., Rodionov D. S., de Souza P. A., Yen A., Gellert R., Evlanov E. N., Foh J., Kankeleit E., Gütlich P., Ming D. W., Renz F., Wdowiak T., Squyres S. W., and Arvidson R. E. 2004. Mineralogy at Gusev crater from the Mössbauer spectrometer on the Spirit Rover. *Science* 305:833–836.

Musselwhite D. S., Dalton H. A., Kiefer W. S., and Treiman A. H. 2006. Experimental petrology of the basaltic shergottite Yamato-980459: Implications for the thermal structure of the Martian mantle. *Meteoritics & Planetary Science* 41:1271–1290.

Mustard J. F., Poulet F., Gendrin A., Bibring J.-P., Langevin Y., Gondet B., Mangold N., Bellucci G., and Altieri F. 2005. Olivine and pyroxene diversity in the crust of Mars. *Science* 307:1594–1597.

Nimmo F. and Tanaka K. 2005. Early crustal evolution of Mars. *Annual Review of Earth and Planetary Sciences* 33:133–161.

Nyquist L. E., Bogard D. D., Shih C.-Y., Greshake A., Stöffler D., and Eugster O. 2001. Ages and geologic histories of Martian meteorites. *Space Science Reviews* 96:105–164.

Ohtani E. and Kamaya N. 1992. The geochemical model of Mars: An estimation from the high-pressure experiments. *Geophysical Research Letters* 19:2239–2242.

Pichavant M., Mysen B. O., and MacDonald R. 2002. Source and H_2O content of high-MgO magmas in island arc settings: An experimental study of a primitive calc-alkaline basalt from St. Vincent, Lesser Antilles arc. *Geochimica et Cosmochimica Acta* 66:2193–2209.

Righter K. and Hauri E. H. 1998. Compatibility of rhenium in garnet during mantle melting and magma genesis. *Science* 280:1737–1741.

Roeder P. L. and Reynolds I. 1991. Crystallization of chromite and chromium solubility in basaltic melts. *Journal of Petrology* 32: 909–934.

Sanloup C., Jambon A., and Gillet P. 1999. A simple chondritic model of Mars. *Physics of the Earth and Planetary Interiors* 112: 43–54.

Sobolev A. and Chaussidon M. 1996. H_2O concentrations in primary melts from supra-subduction zones and mid-ocean ridges: Implications for H_2O storage and recycling in the mantle. *Earth and Planetary Science Letters* 137:45–55.

Squyres S. W., Arvidson R. E., Blaney D. L., Clark B. C.,

Crumpler L., Farrand W. H., Gorevan S., Herkenhoff K. E., Hurowitz J., Kusack A., McSween H. Y., Ming D. W., Morris R. V., Ruff S. W., Wang A., and Yen A. 2006. Rocks of the Columbia Hills. *Journal of Geophysical Research* 111, doi: 10.1029/2005JE002562.

Tormey D. L., Grove T. L., and Bryan W. B. 1987. Experimental petrology of normal MORB near the Kane Fracture Zone: 22–25°N, Mid-Atlantic Ridge. *Contributions to Mineralogy and Petrology* 96:121–139.

Wadhwa M. 2001. Redox state of Mars' upper mantle and crust from Eu anomalies in shergottite pyroxenes. *Science* 291:1527–1530.

Wagner T. P. and Grove T. L. 1997. Experimental constraints on the origin of lunar high-Ti ultramafic glasses. *Geochimica et Cosmochimica Acta* 61:1315–1327.

Zuber M. T., Solomon S. C., Phillips R. J., Smith D. E., Tyler G. L., Aharonson O., Balmino G., Banerdt W. B., Head J. W., Johnson C. L., Lemoine F. G., McGovern P. J., Neumann G. A., Rowlands D. D., and Zhong S. 2000. Internal structure and early thermal evolution of Mars from Mars Global Surveyor topography and gravity. *Science* 287:1788–1793.

APPENDIX

Experimental Data on the Preliminary Gusev Composition

This study was begun on a starting composition that matched the initial rock compositions published for Adirondack, Humphrey, and Mazatzal (McSween et al. 2004). After our study was started, it was discovered that the sensor heads had been inadvertently switched at the launch site, requiring recalibration and recalculation of compositional data for the rocks. The results presented in this paper were based on experiments on the recalibrated composition. The data for the experiments performed on the preliminary composition are presented here for comparison. Table 1 compares the average preliminary and recalibrated composition from McSween et al. (2004) and McSween et al. (2006a). MgO and FeO^* increased and Na_2O decreased in the recalibrated composition, but the changes were generally less than 1 wt% absolute.

The experimental conditions and products for the preliminary composition are presented in Table A1. For the initial composition, the experiments were multiply saturated with olivine, orthopyroxene, and spinel on the liquidus at 1.1 GPa and 1360 °C (Fig. A1), compared to 1.0 GPa and 1320 °C, but the phase relations stayed the same. Opx was still the first crystallizing silicate phase at pressures above multiple saturation, and olivine below. At 0.1 MPa, the appearance temperature for plagioclase and pigeonite was similar for both compositions. Compositional data for the preliminary data set experiments are presented in Table A2.

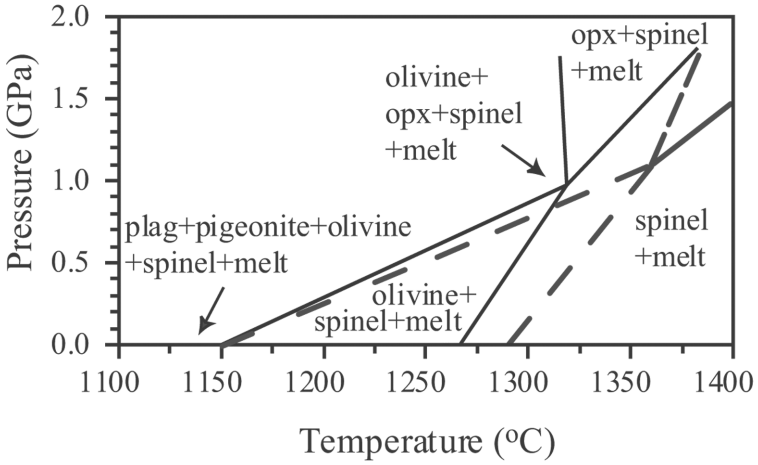

Fig. A1. A comparison of the experimentally determined phase relations for the preliminary (dashed lines) and recalibrated (solid lines) Gusev basalt compositions. An olivine + orthopyroxene + spinel multiple saturation point was found on the liquidus near 1.0 GPa and 1320 °C for the recalibrated composition and near 1.1 GPa and 1360 °C for the preliminary composition.

Table A1. Experimental conditions and products for preliminary Gusev composition.

Run #	Pressure (MPa)	Temp (°C)	Time (h)	Phases[a]	K_D ol/liq	K_D pyx/liq	K_D sp/liq	K_D pl/liq	Mg# gl	Mg# ol	Mg# pyx	Cr# sp	Ca# pl	ΣR^2	ΔFe
GUS-15	0.1 MPa	1125	123	ol (25) + pig (10) + plag (19) + sp (1) + gl (45)	0.35	0.30	1.92	0.74	0.37	0.63	0.67	0.24	0.68	0.56	0.38
GUS-3	0.1 MPa	1195	92	ol + sp + gl	–	–	–	–	–	–	–	–	–	–	–
GUS-4	0.1 MPa	1220	73	ol (12) + sp (2) + gl (84)	0.31	–	1.58	–	0.49	0.76	–	0.38	–	0.69	–3.43
GUS-1	0.1 MPa	1270	24	ol + sp + gl	–	–	–	–	–	–	–	–	–	–	–
GUS-2	0.1 MPa	1300	18	sp + gl	–	–	–	–	–	–	–	–	–	–	–
GUS-5	1.0 GPa	1315	2	ol + opx + sp + gl	–	–	–	–	–	–	–	–	–	–	–
GUS-6	1.0 GPa	1340	2.75	ol + opx + sp + gl	–	–	–	–	–	–	–	–	–	–	–
GUS-11	1.0 GPa	1350	2.25	ol + sp + gl	–	–	–	–	–	–	–	–	–	–	–
GUS-12	1.0 GPa	1370	3	sp + gl	–	–	–	–	–	–	–	–	–	–	–
GUS-9	1.2 GPa	1355	2.25	ol + opx + sp + gl	–	–	–	–	–	–	–	–	–	–	–
GUS-14	1.2 GPa	1375	2.5	sp + gl	–	–	–	–	–	–	–	–	–	–	–
GUS-8	1.5 GPa	1380	2.25	opx + sp + gl	–	–	–	–	–	–	–	–	–	–	–
GUS-10	1.5 GPa	1400	2.25	opx + sp + gl	–	–	–	–	–	–	–	–	–	–	–
GUS-13	1.5 GPa	1420	2	sp + gl	–	–	–	–	–	–	–	–	–	–	–

[a]Abbreviations: gl = glass; ol = olivine; pyx = pyroxene (including opx = orthopyroxene and pig = pigeonite); sp = spinel. Phase proportions calculated by mass balance.

Table A2. Electron microprobe analyses of phases produced in 0.1 MPa experiments on the preliminary Gusev composition.

Run #	Phase[a]	SiO_2	TiO_2	Al_2O_3	Cr_2O_3	FeO	MnO	MgO	CaO	Na_2O	K_2O	P_2O_5	Total
GUS-15	gl (12)	50.2 (6)	0.95 (8)	12.3 (2)	0.06 (2)	17.0 (4)	0.37 (3)	5.67 (14)	10.2 (1)	1.99 (10)	0.10 (1)	0.98 (12)	99.84
	ol (7)	36.6 (6)	–	–	–	32.3 (2)	0.60 (2)	30.2 (3)	0.41 (2)	–	–	–	100.09
	pig (7)	52.6 (3)	0.17 (2)	1.29 (5)	0.49 (2)	18.7 (3)	0.58 (2)	21.0 (5)	5.75 (67)	0.07 (3)	–	–	100.67
	pl (7)	52.1 (6)	–	29.3 (7)	–	1.23 (25)	–	0.38 (16)	13.6 (3)	3.53 (19)	0.04 (1)	–	100.18
	sp (7)	0.39 (18)	2.73 (75)	16.5 (1.6)	35.7 (4.1)	36.7 (2.2)	0.43 (2)	6.28 (31)	0.27 (4)	–	–	–	100.03
GUS-3	gl (9)	49.7 (2)	0.55 (5)	13.1 (1)	0.01 (1)	16.2 (1)	0.39 (3)	8.14 (6)	9.42 (4)	1.17 (6)	0.07 (1)	0.55 (6)	99.30
	ol (3)	37.8 (2)	–	–		23.0 (1)	0.46 (2)	38.5 (1)	0.40 (11)	–	–	–	100.05
GUS-4	gl (9)	49.3 (3)	0.52 (5)	12.8 (1)	0.02 (3)	16.6 (2)	0.38 (3)	9.03 (13)	9.11 (8)	1.30 (9)	0.07 (1)	0.58 (6)	99.66
	ol (3)	38.5 (5)	–	–	–	22.1 (3)	0.39 (3)	38.8 (8)	0.29 (2)	–	–	–	100.02
	sp (3)	0.20 (15)	0.31 (4)	20.3 (3)	41.8 (8)	26.7 (2)	0.26 (4)	9.22 (22)	0.13 (4)	–	–	–	99.63
GUS-1	gl (9)	47.9 (3)	0.48 (6)	11.8 (1)	0.05 (2)	17.3 (2)	0.38 (3)	10.8 (1)	8.44 (9)	1.61 (7)	0.07 (1)	0.50 (4)	99.24
	ol (3)	38.3 (2)	–	–	–	20.1 (1)	0.40 (5)	41.7 (2)	0.31 (1)	–	–	–	100.79
GUS-2	gl (9)	47.4 (2)	0.44 (3)	11.2 (1)	0.12 (2)	17.5 (2)	0.39 (2)	12.6 (1)	8.01 (10)	1.42 (10)	0.06 (1)	0.46 (5)	99.57

[a]Abbreviations: gl = glass; ol = olivine; pyx = pyroxene (including opx = orthopyroxene and pig = pigeonite); sp = spinel. Phase proportions calculated by mass balance.